

Signatures for multifragmentation in spallation reactions

Karl-Heinz Schmidt for the CHARMS collaboration*
GSI, Planckstr. 1, D-64291 Darmstadt, Germany

Abstract: The traditional theoretical description of spallation reactions by intra-nuclear cascade codes, pre-equilibrium-emission models and evaporation codes disregards phenomena related to the thermal expansion of the excited system. When the system is sufficiently heated, a simultaneous decomposition of the expanded system into several fragments occurs, which is interpreted as a manifestation of spinodal instabilities in the dynamic evolution of the system. Some salient experimental signatures of this multifragmentation phenomenon are described.

1. Introduction

Multifragmentation, i.e. high-multiplicity emission of intermediate-mass fragments ($3 \leq Z \leq 30$), has been observed in spallation reactions with cosmic rays nearly seventy years ago [1]. The fragments were considerably smaller than typical fission products and larger than typical evaporation products. At present, multifragmentation induced by spallation is still subject of intense fundamental research [2] on the equation of state of nuclear matter and liquid-gas phase transition in nuclear matter. In contrast to heavy-ion collisions, where the experimental observables and theoretical description are complicated by effects such as compression and/or shape distortion, spallation reactions are characterised by pure thermal excitations. Thus, spallation reactions provide unique conditions for studying the evolution of a heated nuclear system.

The scenario thought to be responsible for thermal multifragmentation is the expansion of the hot system due to thermal pressure [3], which brings the system into spinodal unstable conditions [4]. The expanding system divides simultaneously into several fragments and single nucleons [5].

The experimental features invoked as signatures for multifragmentation are manifold, but their interpretation is often rather complex:

1. High multiplicities of IMFs [6].
2. High cross sections for light fragments.
3. Short emission times (for multiplicity > 2) [7, 8].
4. Large slope parameters in the emission energy spectra [9, 10].
5. Large fluctuations in folding-angle distributions of fission fragments [11].
6. Plateau-like behaviour of the caloric curve [12].
7. Large fluctuations in momentum distributions from invariant cross sections [13].

While some signatures, e.g. short emission times, give rather direct evidence for multifragmentation, many of the other observables may be described with models based on different scenarios, possibly after adjusting some model parameters, or they are dominated by other effects, not related to multifragmentation. Another complication is given by the contribution of pre-equilibrium processes [14].

It is particularly difficult to identify multifragmentation near its threshold [15]. The importance of the momentum or energy distributions of the fragments as one of the clearest signatures of multifragmentation, which reflects the volume and the thermal expansion of the emitting source, has recently been stressed [13, 16].

* <http://www.gsi.de/charms>

In technical applications of spallation reactions, it is important to consider nuclear expansion and multifragmentation, in order to obtain realistic and complete model predictions for the yields and the kinematical properties of the different reaction products.

2. Conventional description of spallation reactions

The model description of the spallation process, which is most often used and which has proven to be quite successful in reproducing most of the observations consists of two or three separate stages: firstly, a semi-classical description of the nuclear-collision phase, secondly, eventually a separate process of pre-equilibrium particle emission and thermal equilibration and, finally, a statistical description of the de-excitation phase. The first phase is described as a sequence of individual nucleon-nucleon collisions. In this process, the incoming nucleon distributes part of its kinetic energy to a number of nucleons. Some of these leave the system, while the target nucleus is left with several holes and excited particles on the single-particle levels. Codes of this type are called intra-nuclear cascades. Some examples are the Bertini code [17], which has traditionally been used in applications of nuclear technology, or the more recent codes like e.g. ISABEL [18], the Toneev INC code [19] and INCL [20]. In spite of its classical basics, additional effects like the influence of Fermi motion and excitations of the nucleon are considered. In case the intra-nuclear cascade is stopped before thermal equilibrium is reached, an intermediate stage of thermalisation is considered, in which the system passes by more and more complex single-particle configurations, and in which particles which acquire energies above the continuum may leave the system, e.g. refs. [21, 22]. The last stage is modelled by a conventional evaporation code, where the emission of nucleons and light nuclei, fission and gamma radiation is treated as a compound-nucleus decay.

3. Scenario of thermal multifragmentation

In the above-mentioned conventional description of the spallation process, the nuclear density is not considered as a degree of freedom of the system. All reaction stages were assumed to proceed at normal nuclear density. However, if we consider the variation of the potential energy and the variation of the level density as a function of nuclear density, the most probable shape of a heated nucleus is found at reduced nuclear density.

In order to illustrate this behaviour, a schematic calculation was performed. It was assumed that the compression energy E_c follows a parabola as a function of density. It is set to zero at normal nuclear density ρ_0 :

$$E_c = K \cdot (\rho - \rho_0)^2$$

The nuclear level density ω is formulated as

$$\omega \propto \exp\left(2\sqrt{a(E - E_c)}\right).$$

Following the relations of the Fermi gas, the level-density parameter a also depends on the density ρ and the volume V , respectively:

$$a \propto \rho^{-1} \propto V$$

The result is illustrated in figure 1. The most probable volume of a heated nucleus is given by the maximum entropy $S = \ln(\omega)$ for fixed excitation energy E of the system. The schematic model clearly shows that the nucleus tends to expand when it is heated.

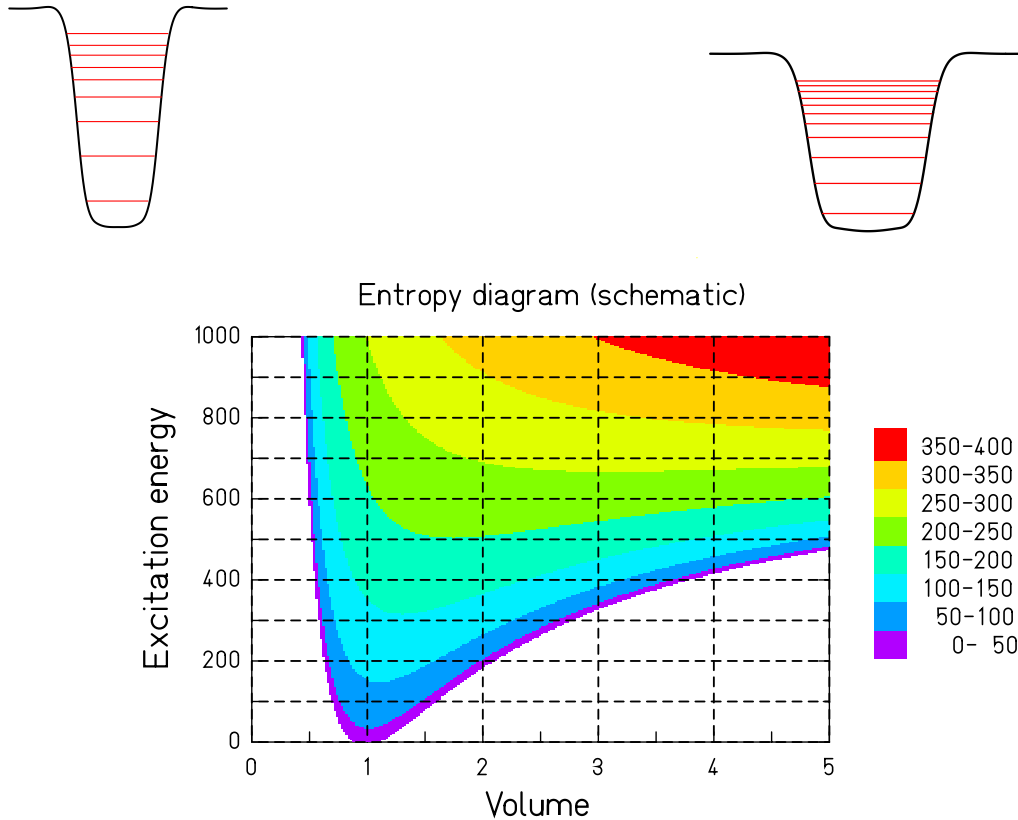


Fig. 1: Schematic entropy diagram of a heated nucleus as a function of its volume relative to normal nuclear density. When the nucleus expands, the binding energy decreases, but the density of single-particle levels increases (see upper insets). The most probable volume, which is given by the maximum entropy for a given energy of the system, grows if the nucleus is heated.

In a spallation process, the nucleus is heated during the short nuclear collision stage and feels a driving force towards expansion due to the gradient of the entropy. In this process, the nucleus might enter into a region of spinodal instability. That means by lowering the density, the nuclear matter divides into two phases, drops of liquid with normal density, corresponding to intermediate-mass fragments, and a gas of individual nucleons [4]. This process is qualitatively similar to the boiling of hot water when the pressure is reduced. After break-up, the system explodes due to the repulsive Coulomb forces between the fragments as sketched in the schematic drawing of figure 2. The size distribution of the fragments has been estimated by phase-space arguments in the statistical multifragmentation model (SMM) [5], where all possible partitions are considered and weighted by the number of available states.

A more detailed report on the theoretical understanding of the multifragmentation phenomenon is given in the contribution of A. Botvina [23] to this conference.

The major scientific interest in the multifragmentation process relies in the relation to the equation of state of nuclear matter and in particular to the liquid-gas phase transition. The practical relevance for nuclear technology lies in the enhanced yields of intermediate-mass fragments and their specific kinematic properties.

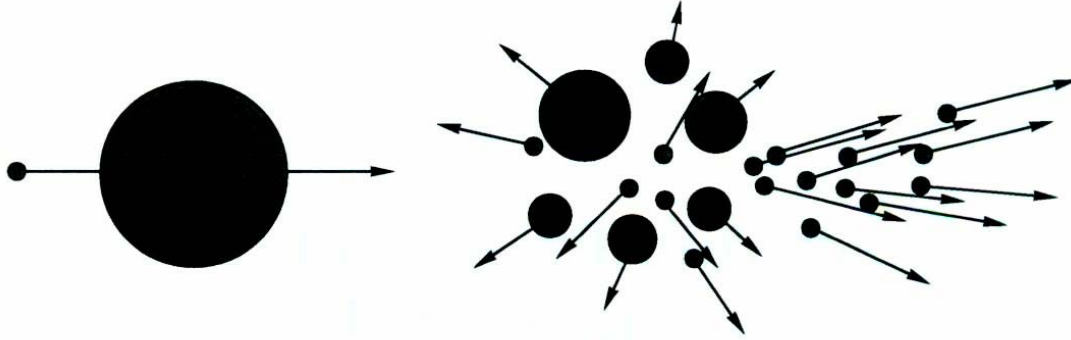


Fig. 2: Picture of the break-up of a heavy target nucleus in many fragments after the bombardment with a high-energetic proton (from ref. [2]).

4. Experimental signatures

In the present contribution, we consider three classes of observables as experimental signatures of multifragmentation:

- Emission times
- Mass spectra
- Kinematical properties

Experimental results on emission times prove most clearly that the conventional picture of the spallation reaction, in particular the evaporation picture of the deexcitation process is not adapted if the energy deposited in the intra-nuclear-cascade phase exceeds a certain value. Specific characteristics of yield and multiplicity distributions as well as the kinematics have important consequences for applications. They have been investigated with several experimental methods. We will discuss the results in the following sub-sections.

4.1. Emission times

In many spallation reactions, several fragments are observed in the same event. This observation gave the name to the multifragmentation process. However, this observation alone does not prove, whether the fragments are produced in a simultaneous break-up of the excited system or whether the fragments origin from a sequence of binary decays, since the emission times in the evaporation process of a highly excited nucleus are so short that they cannot directly be measured. On the other hand, the Coulomb repulsion between simultaneously emitted fragments deflects them if they are, by chance, emitted in the same direction in space. Therefore, the angular correlation of fragments emitted in the same event yields the desired information on the time scale of the emission process. Figure 3 proves that the emission of intermediate-mass fragments (IMFs) in the reaction ${}^4\text{He} + {}^{197}\text{Au}$ at 3.65 A GeV originates essentially from the simultaneous decay of the excited system.

This detailed feature of the distribution of relative angles of the emitted fragments has little direct influence on technical applications of the spallation process. However, it has fundamental importance for our understanding of the physics and for the development of codes which model the creation of intermediate-mass fragments in spallation reactions in a realistic way.

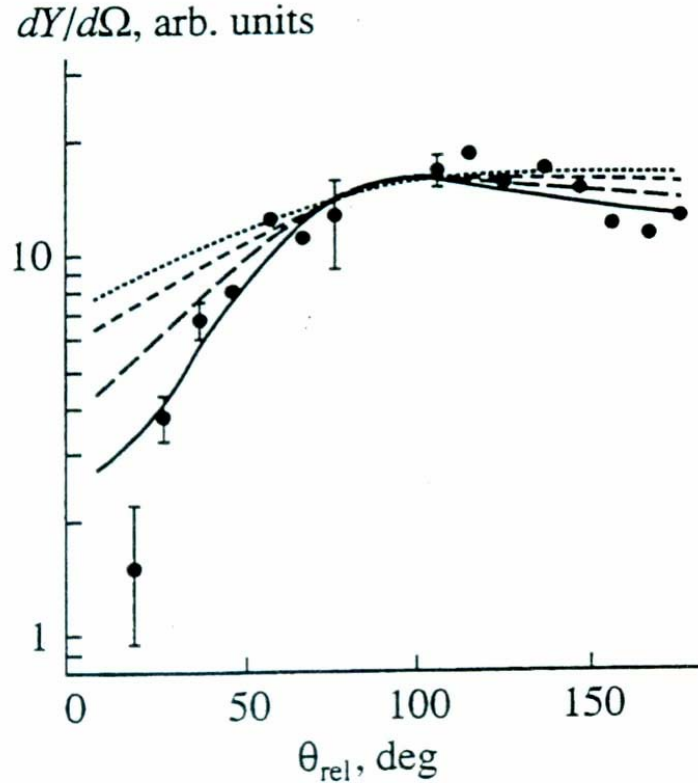


Figure 3: Distribution of relative angles between IMFs ($6 \leq A \leq 30$) observed in the reaction $^{197}\text{Au} + ^4\text{He}$ at $E = 3.65 A$ GeV. The dots are experimental data. The curves are calculated for different mean lifetimes τ of the fragmenting system: (solid line) $\tau = 0$, (dashed line) $\tau = 100$ fm/c, and (two remaining lines) $\tau = 400$ and 800 fm/c (from ref. [7]).

4.2 Mass yields

From many experiments, one has deduced that the production cross sections in the domain of multifragmentation follow a power law

$$\frac{d\sigma}{dA} \propto A^{-\tau}$$

Figure 4 shows the mass distribution observed in the reaction $^4\text{He} + ^{197}\text{Au}$ at $3.6 A$ GeV from ref. [2]. At low multiplicity, the additional contribution from fission clearly appears around mass 80. Almost independently of the multiplicity, the mass distribution of intermediate-mass fragments is well described by a power law with an exponent $\tau \approx 2$. The value of τ turned out to be rather universal.

These mass spectra can be reproduced with the statistical multifragmentation model (SMM) if the critical temperature of the phase diagram of nuclear matter is set to $T_c = 20 \pm 3$ MeV and the density of the expanded source at fragment formation is set to $1/3$ of normal nuclear density [24].

The characteristics of the mass yields emerging from collisions of ^{208}Pb projectiles with different targets have been determined over a large range of collision energies in an inclusive experiment [25]. At low energies ($^{208}\text{Pb} + ^1\text{H}$, $1 A$ GeV), only heavy spallation products and fission fragments are produced. At higher energies, the production of light and intermediate-

mass fragments grows, while the relative production of fission and heavy products decreases. One should mention that the production of fission products appearing in $^{208}\text{Pb} + ^{208}\text{Pb}$ collisions at the highest energy (158 A GeV) is mostly caused by electromagnetic excitations.

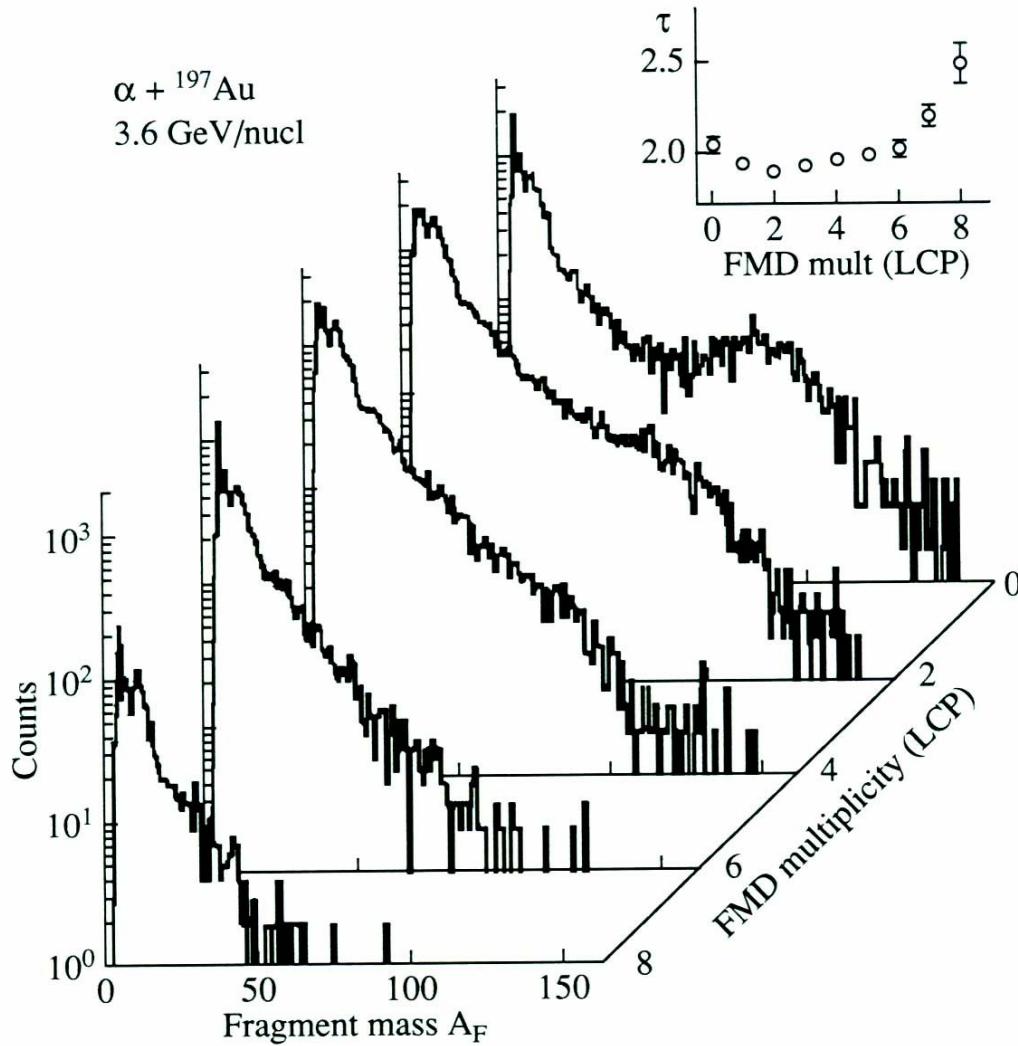


Figure 4: Mass spectra for $^4\text{He} + ^{197}\text{Au}$ at 3.6 A GeV collisions measured as function of the multiplicity of light charged particles. The inset gives the power-law parameter τ , deduced from the mass spectrum in the region $10 \leq A \leq 40$ (from ref. [2]).

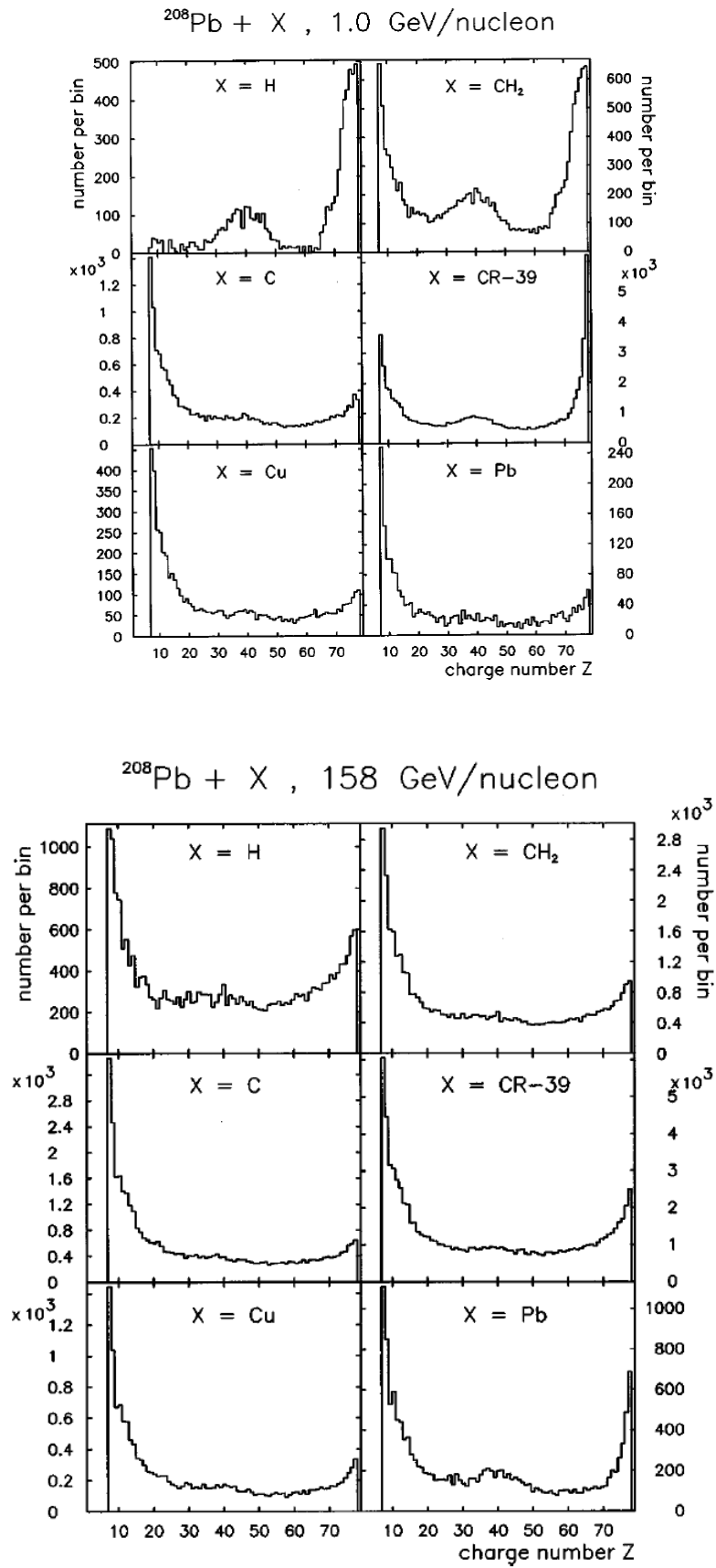


Fig. 5: Yield spectra for the charges of fragments measured for reactions of ^{208}Pb projectiles with H, CH_2 , C, CR-39, Cu, and Pb at beam energies of 1 A GeV (upper part) and 158 A GeV (lower part), from ref. [25].

4.3 Nuclide cross sections

The powerful installations of GSI, Darmstadt, in particular the heavy-ion synchrotron SIS18 and the magnetic spectrometer FRS were used to introduce a novel experimental approach, which allowed for the first time to determine the full nuclide distribution produced in spallation reactions. The main feature is the study of projectile-like fragments with a high-resolution magnetic spectrometer to identify the reaction products in-flight. This means that a high-energy beam of the nucleus to be investigated impinges on a hydrogen target. Thus, the reaction products can be analysed in flight, allowing for a full identification in nuclear charge Z and mass number A of all products. Figure 6 shows a sequence of nuclide distributions from the spallation of ^{208}Pb at 0.5, 1 and 2 GeV by protons, respectively deuterons. These data clearly reveal the different N/Z ratio of spallation-evaporation and spallation-fission products. While spallation-fission products from this reaction are situated close to beta-stability, spallation evaporation products are shifted to the proton-rich side. During the last years, several systems were investigated by a collaboration of scientists from Santiago de Compostela (Spain), CEA Saclay (France), IPN Orsay (France) and GSI Darmstadt in an experimental campaign. More details on these experiments are presented in the contribution of A. Kelić [26] to this conference.

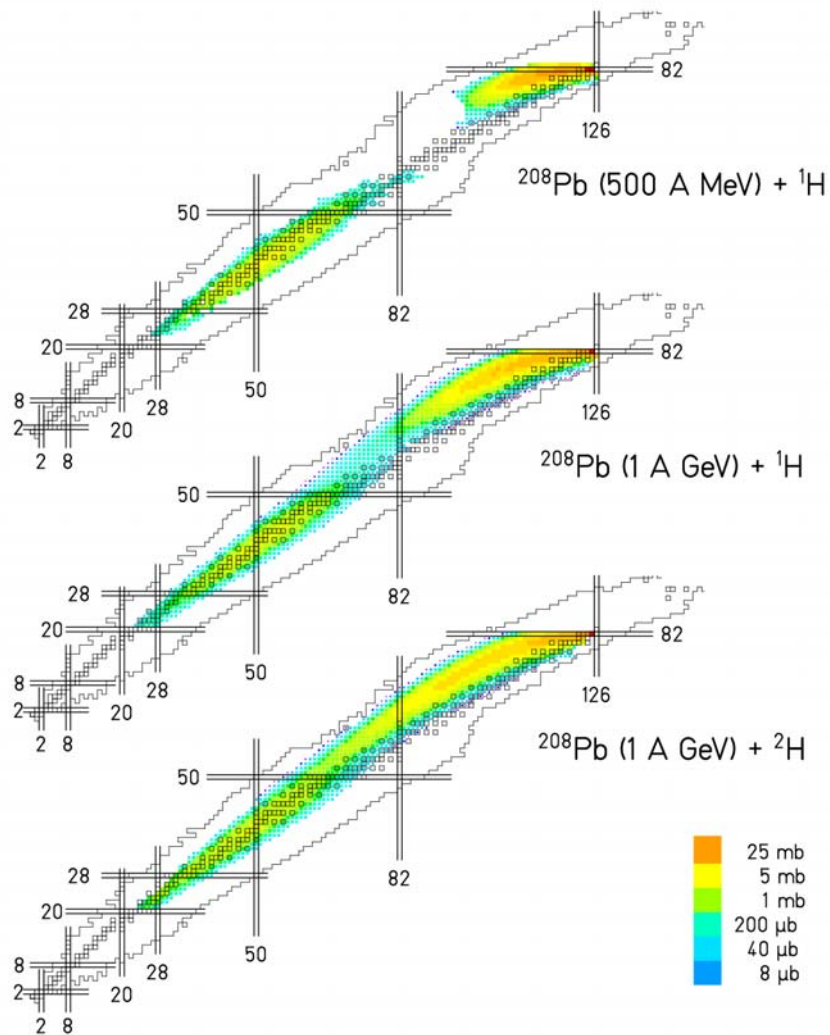


Fig. 6: Nuclide distributions from the spallation of ^{208}Pb by protons of 0.5 and 1 GeV and by deuterons of 2 GeV measured using the inverse-kinematics approach at GSI, Darmstadt [27, 28, 29, 30].

4.4 Kinematics

Before discussing the expected kinematical properties of fragments emerging from the break-up of a hot expanding source, it is very instructive to first consider the case of evaporation from complete-fusion reaction products. Also the first interpretations of measured kinetic-energy and momentum distributions in spallation reactions were guided by the experience in this field.

In complete fusion, the amalgamated system carries precisely the total momentum of the projectile, and no additional fluctuations occur. The kinetic-energy spectra of the evaporated particles and fragments are described by a Maxwell-Boltzmann distribution

$$\frac{d\sigma}{d\varepsilon} \propto \varepsilon \cdot e^{-\varepsilon/T}$$

with a slope parameter T determined by the inverse logarithmic slope of the level density of the daughter nucleus [31] as a function of its excitation energy, equivalent to the temperature of the daughter nucleus. The evaporation process is completely governed by the phase space of the “final” state, i.e. the configuration when the emitted particle leaves the system. The reason is that evaporation is a “rare” process compared to the lifetime of a certain intrinsic configuration of the excited system. This result is analogue to the thermal evaporation spectrum of molecules from a liquid.

When considering the kinetic-energy or momentum distributions of spallation residues, there are some important differences, which induce some additional fluctuations in the kinematics of the system. *Firstly*, the excited thermalised system left over after the INC stage receives only part of the momentum of the interacting nucleon, which in addition is subject to fluctuations. *Secondly*, the individual nucleons in the heavy reaction partner, which are involved in the collisions with the incoming nucleon in the INC stage, are subject to the Fermi motion. Even at zero excitation energy, the Fermions are packed in single-particle levels in the potential-energy well up to the Fermi level. The Fermi motion of a colliding nucleon on its individual energy level enters into the kinematics of the nucleon-nucleon collision. Also the Pauli exclusion principle must be considered for the possible final states after the collision. Therefore, the source emerging from an INC process is subject to substantial fluctuations in momentum, which must be considered when interpreting the kinematical properties of the final spallation products. Due to the many contributing individual processes, the momentum distribution in space should resemble a 3-dimensional Gaussian in space. It is interesting to note that this transforms into an energy distribution of the kind

$$\frac{dI}{d\varepsilon} \propto \sqrt{\varepsilon} \cdot e^{-\varepsilon/\tau}$$

which has a functional form very similar to the Maxwell-Boltzmann distribution of evaporated particles. In particular, both show an exponential tail towards high kinetic energies. In case of evaporation from a spallation pre-fragment, the distributions created by the two processes should be convoluted. Thus, the high-energy part of the measured energy distribution shows a decreased logarithmic slope, and thus the slope parameter cannot be interpreted as a temperature any more.

The kinematics of fragments emitted by thermal multifragmentation from this source according to the scenario described above might be described by the following schematic picture: The fragments are homogeneously distributed over the volume of the expanding source. They move with the sum of the Fermi momenta of their constituents. It should be considered that the Fermi momentum is reduced compared to normal nuclei if the volume of

the source is increased. At a certain moment, called freeze-out, the nuclear interactions between the fragments become negligible, and the further kinematics is determined by the Coulomb force alone. The kinematics of the fragments after acceleration may be estimated by the Wigner-Seitz approximation. To get a rough idea on the magnitude of the kinetic energy induced on the Coulomb trajectory, we consider a fragment emitted from the surface of a spherical source with zero initial velocity. It will acquire a kinetic energy

$$E_{kin} = \frac{e^2 Z_f (Z_{source} - Z_f)}{r_{source}}$$

The probability to meet the fragment at another distance r from the centre of the source varies proportional to r^2 . Geometrical considerations yield that the shape of the kinetic-energy spectrum is like $dn/dE \propto \sqrt{E}$, and the velocity profile in beam direction (invariant cross section) is $dn/dv_{\parallel} = const.$ up to the extreme values. Altogether, the distribution of momenta in the three-dimensional space is the convolution of a spherical homogeneous distribution due to the Coulomb repulsion with a three-dimensional Gaussian due to the Fermi momentum of the constituents of the fragments. The Gaussian contribution creates a tail in the energy distribution with an apparent “temperature” as high as about 15 MeV [32]. In addition, a radial-flow velocity at freeze-out adds up to the final velocities of the fragments.

Figure 7 shows the energy spectra of light charged particles from the reaction Au + Au at 1 A GeV [10] measured at GSI with the ALADIN large-acceptance dipole magnet. The apparent temperature values deduced from the slopes of these spectra, figure 8, are found to be slightly larger than 15 MeV, while the nuclear temperatures at freeze-out deduced from isotopic ratios are appreciably smaller, around 5 to 6 MeV. This discrepancy reveals the difficulty to interpret the slope parameter as a temperature value.

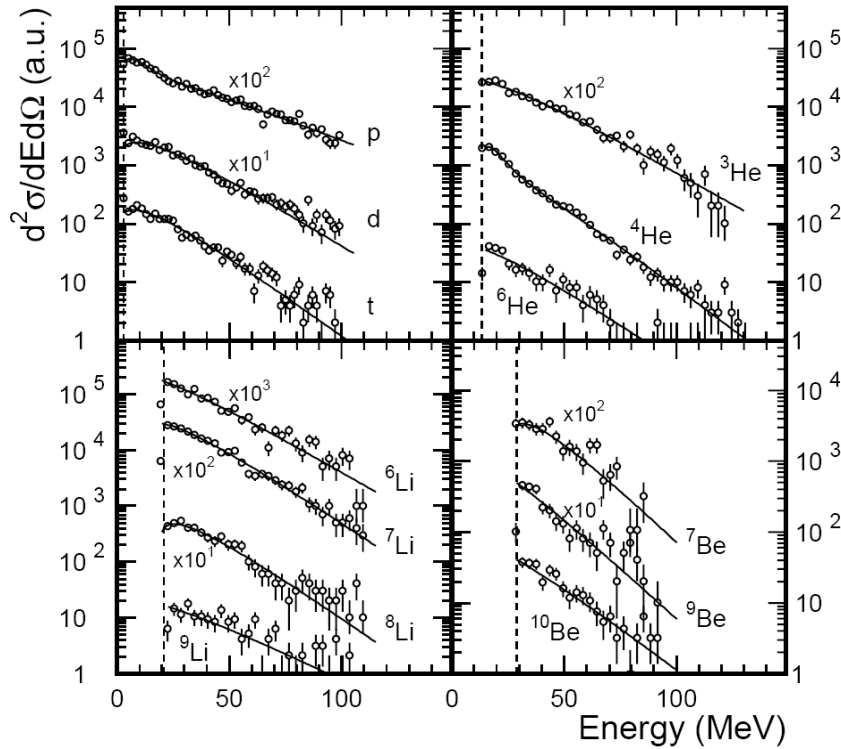


Fig. 7: Energy spectra of light charged particles and fragments with $Z \leq 4$ at 150° , integrated over $20 \leq Z_{bound} \leq 60$ from the reaction Au + Au at 1 A GeV, from ref. [10].

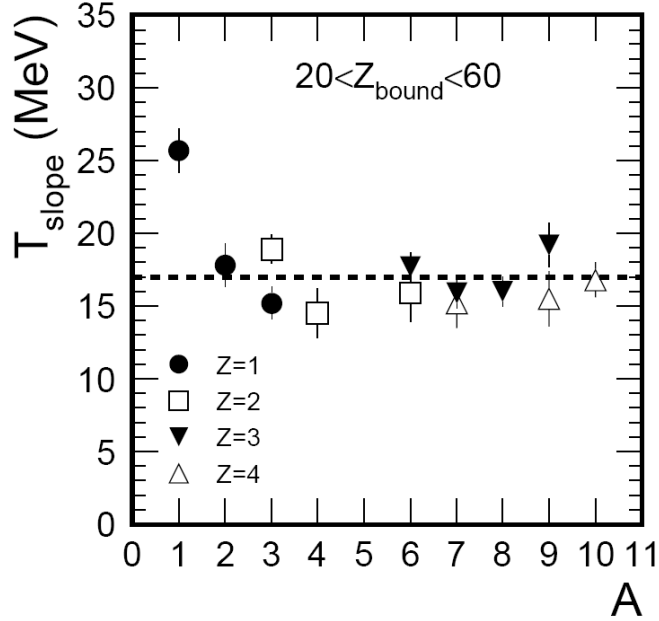


Fig. 8: Slope parameters for isotopically resolved charged particles and fragments as a function of mass number A , from ref. [10].

We state that the kinematical properties of multifragmentation products are subject to several sources of fluctuations in velocity, respectively energy. Therefore, the interpretation of the measured characteristics of the kinematics in multifragmentation is rather complex.

High-resolution experiments performed with the FRS spectrometer revealed even more complex features of the velocity spectra of intermediate-mass fragments produced in spallation and fragmentation reactions, see fig. 9. One can distinguish two components: a double-humped distribution dominates for the lightest products in proton-induced reactions, which induce the lowest energies and a single-humped distribution takes over for the heavier products and for the systems with higher energy introduced. Fragments observed in the double-humped distribution seem to originate from the decay of a heavy system with one heavy remnant. The Coulomb repulsion from the heavy remnant causes the velocity spread between the forward and backward component of the light fragment we observe. Events in the single-humped distribution may originate from the decay in fragments of similar size. In addition, the two components appear at different mean velocity, revealing that they originate from different emitting systems. Due to a systematic study of the momentum transfer induced in the abrasion process [33], the fragments in the double-humped distribution stem from rather peripheral collisions, while the fragments in the single-humped distribution originate from much more central collisions. This topic will be discussed in more detail in the contribution of P. Napolitani [34] to this conference.

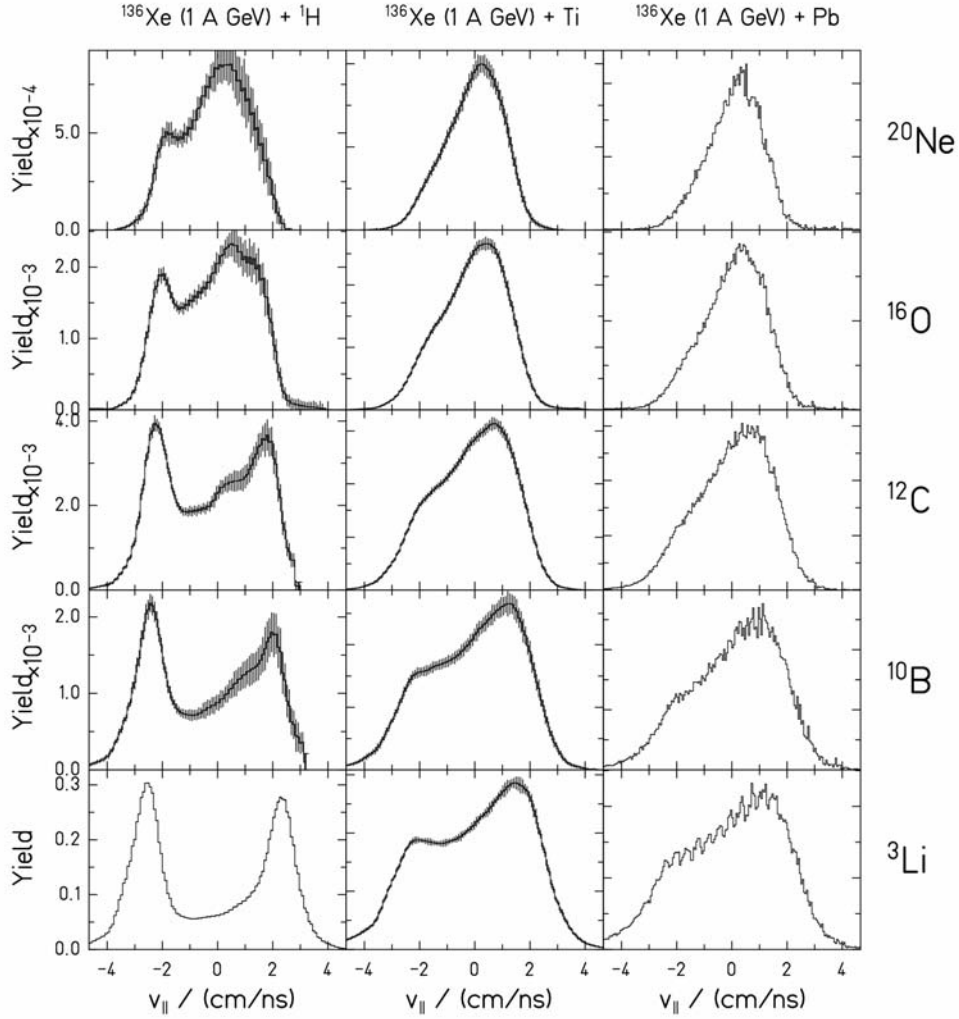


Fig. 9: Longitudinal velocity distributions of fragments emitted close to the beam direction produced in the collisions of ^{136}Xe with protons, titanium and lead at 1 A GeV [35, 36].

5. Conclusion

Spallation reactions, which are defined as collisions of high-energy particles, e.g. protons, with heavy nuclei, produce a large number of light fragments. When the system is sufficiently heated, the simultaneous emission of intermediate-mass fragments (IMFs) occurs. They are heavier than typical evaporation products and lighter than typical fission fragments. Conventional nuclear-reaction codes, consisting of intranuclear-cascade, pre-equilibrium emission and an evaporation-fission model, fail to model the multifragmentation process. Additional features like thermal expansion and liquid-gas instabilities are thought to be responsible for the multifragmentation phenomenon.

Powerful experimental approaches have been introduced at GSI Darmstadt, using the ALADIN dipole magnet and the FRS magnetic spectrometer, which allow for large-acceptance experiments and high-resolution measurements of the fragmentation products, respectively.

The kinematics of these multifragmentation products is rather complex: Apparent temperatures are rather high and inconsistent with temperatures deduced by other methods. The velocity spectra of the lightest fragments show a substructure, revealing the production of the same nuclides by at least two different sources and two different processes.

-
- [1] *E. Schopper*, *Naturwiss.* **25** (1937) 557.
- [2] *V. A. Karnaukov*, *Phys. of Part. and Nuclei* **37** (2006) 165.
- [3] *P. J. Siemens*, *Nature* **305** (1983) 410.
- [4] *Ph. Chomaz, M. Colonna, J. Randrup*, *Phys. Rep.* **389** (2004) 263.
- [5] *J. P. Bondorf, A. S. Botvina, A. S. Iljinov, I. N. Mishustin, K. Sneppen*, *Phys. Rep.* **257** (1995) 133.
- [6] *C. A. Ogilvie et al.*, *Phys. Rev. Lett* **67** (1991) 1214.
- [7] *S. Yu. Shmakov et al.*, *Phys. Atom. Nuclei* **58** (1995) 1635.
- [8] *L. Beaulieu et al.*, *Phys. Rev. Lett.* **84** (2000) 5971.
- [9] *G. D. Westfall et al.*, *Phys. Rev. C* **17** (1978) 1368.
- [10] *T. Odeh et al.*, *Phys. Rev. Lett.* **84** (2000) 4557.
- [11] *H. W. Barz et al.*, *Nucl. Phys. A* **460** (1986) 714.
- [12] *J. Pochodzalla et al.*, *Phys. Rev. Lett.* **75** (1995) 1040.
- [13] *P. Napolitani et al.*, *Phys. Rev. C* **70** (2004) 054607.
- [14] *S. Turbide et al.*, *Phys. Rev. C* **70** (2004) 014608.
- [15] *M. V. Ricciardi et al.*, *Phys. Rev. C* **73** (2006) 014607.
- [16] *S. G. Mashnik, K. K. Gudima, M. I. Baznat*, arXiv: nucl-th/0603046.
- [17] *H. W. Bertini*, *Phys. Rev.* **131** (1963) 1801.
- [18] *Y. Yariv, Z. Fraenkel*, *Phys. Rev. C* **24** (1981) 488.
- [19] *V. D. Toneev, K. K. Gudima*, *Nucl. Phys. A* **400** (1973) 173c.
- [20] *A. Boudard, J. Cugnon, S. Leray, C. Volant*, *Phys. Rev. C* **66** (2002) 044615.
- [21] *M. Blann, M. B. Chadwick*, *Phys. Rev. C* **62** (2000) 034604.
- [22] *C. Kalbach*, *Phys. Rev. C* **73** (2006) 024614.
- [23] *A. Botvina*, contribution to this conference.
- [24] *V. A. Karnaukhov et al.*, *Nucl. Phys. A* **734** (2004) 520.
- [25] *G. Hüntrup et al.*, *Phys. Rev. C* **61** (2000) 034903.
- [26] *A. Kelic*, contribution to the conference.
- [27] *T. Enqvist et al.*, *Nucl. Phys. A* 686 (2001) 481.
- [28] *T. Enqvist et al.*, *Nucl. Phys. A* 703 (2002) 435.
- [29] *B. Fernandez et al.*, *Nucl. Phys. A* 747 (2005) 227.
- [30] *L. Audouin et al.*, *Nucl. Phys. A* 768 (2006) 1.
- [31] *V. F. Weisskopf*, *Phys. Rev.* **52** (1937) 295.
- [32] *A. S. Goldhaber*, *Phys. Lett.* **B 53** (1974) 306.
- [33] *V. Henzl*, PhD thesis, Czech Technical University Prague, 2006.
- [34] *P. Napolitani*, contribution to this conference.
- [35] *P. Napolitani*, PhD thesis, Université Paris XI, 2004.
- [36] *D. Henzlova*, PhD thesis, Czech Technical University Prague, 2006.